Redox Biology 41 (2021) 101951

Contents lists available at ScienceDirect

Redox Biology

journal homepage: www.elsevier.com/locate/redox

Sulforaphane exposure impairs contractility and mitochondrial function in three-dimensional engineered heart tissue

Alexandra Rhoden [a,b,**], Felix W. Friedrich [a,b], Theresa Brandt [c], Janice Raabe [a,b], Michaela Schweizer [d], Jana Meisterknecht [e], Ilka Wittig [e], Bärbel M. Ulmer [a,b], Birgit Klampe [a,b], June Uebeler [a,b], Angelika Piasecki [a,b], Kristina Lorenz [c,f], Thomas Eschenhagen [a,b], Arne Hansen [a,b], Friederike Cuello [a,b,*]

[a] Institute of Experimental Pharmacology and Toxicology, Cardiovascular Research Center, University Medical Center Hamburg-Eppendorf, Martinistrasse 52, 20246, Hamburg, Germany
[b] DZHK (German Center for Cardiovascular Research), Partner Site Hamburg/Kiel/Lübeck, University Medical Center Hamburg-Eppendorf, Martinistrasse 52, 20246, Hamburg, Germany
[c] Institute of Experimental Pharmacology and Toxicology, University of Würzburg, Versbacher Str., 9 97078, Würzburg, Germany
[d] Department of Morphology and Electron Microscopy, Center for Molecular Neurobiology, University Medical Center Hamburg-Eppendorf, 20246, Hamburg, Germany
[e] Functional Proteomics, Faculty of Medicine, Goethe University Frankfurt, 60590, Frankfurt, Germany
[f] Leibniz-Institut für Analytische Wissenschaften – ISAS e.V., Bunsen-Kirchhoff-Str. 11, 44139, Dortmund, Germany

ARTICLE INFO

Keywords:
Sulforaphane
Engineered heart tissue
Contractile and mitochondrial function

ABSTRACT

Sulforaphane (SFN) is a phytochemical compound extracted from cruciferous plants, like broccoli or cauliflower. Its isothiocyanate group renders SFN reactive, thus allowing post-translational modification of cellular proteins to regulate their function with the potential for biological and therapeutic actions. SFN and stabilized variants recently received regulatory approval for clinical studies in humans for the treatment of neurological disorders and cancer. Potential unwanted side effects of SFN on heart function have not been investigated yet. The present study characterizes the impact of SFN on cardiomyocyte contractile function in cardiac preparations from neonatal rat, adult mouse and human induced-pluripotent stem cell-derived cardiomyocytes. This revealed a SFN-mediated negative inotropic effect, when administered either acutely or chronically, with an impairment of the Frank-Starling response to stretch activation. A direct effect of SFN on myofilament function was excluded in chemically permeabilized mouse trabeculae. However, SFN pretreatment increased lactate formation and enhanced the mitochondrial production of reactive oxygen species accompanied by a significant reduction in the mitochondrial membrane potential. Transmission electron microscopy revealed disturbed sarcomeric organization and inflated mitochondria with whorled membrane shape in response to SFN exposure. Interestingly, administration of the alternative energy source L-glutamine to the medium that bypasses the uptake route of pyruvate into the mitochondrial tricarboxylic acid cycle improved force development in SFN-treated EHTs, suggesting indeed mitochondrial dysfunction as a contributor of SFN-mediated contractile dysfunction. Taken together, the data from the present study suggest that SFN might impact negatively on cardiac contractility in patients with cardiovascular co-morbidities undergoing SFN supplementation therapy. Therefore, cardiac function should be monitored regularly to avoid the onset of cardiotoxic side effects.

1. Introduction

Sulforaphane (SFN) is a phytochemical compound that can be extracted from cruciferous plants, like broccoli or cauliflower. It has an isothiocyanate (ITC) group, which renders SFN reactive allowing modulation of cellular protein [1]. Thereby, the positively charged carbon in the ITC group can elctrophilically adduct to nucleophilic protein

* Corresponding author. Institute of Experimental Pharmacology and Toxicology; University Medical Center Hamburg-Eppendorf, Martinistrasse 52; 20246, Hamburg, Germany.
** Corresponding author. Institute of Experimental Pharmacology and Toxicology; University Medical Center Hamburg-Eppendorf, Martinistrasse 52; 20246, Hamburg, Germany.
E-mail addresses: dralexandra.rhoden@gmail.com (A. Rhoden), f.cuello@uke.de (F. Cuello).

https://doi.org/10.1016/j.redox.2021.101951
Received 18 February 2021; Received in revised form 16 March 2021; Accepted 16 March 2021
Available online 31 March 2021

thiolates and alter structure and function of proteins. Consequently, it can also change the activity of transcription factors (like KEAP1/Nrf2) and has been described to act as a strong indirect antioxidan [2–4].

List of abbreviations

AAV	Adeno-associated viral vector
BN-PAGE	Blue native polyacrylamide gel electrophoresis
CM	Cardiomyocytes
DMSO	Dimethylsulfoxid
EHT	Engineered heart tissue
$FADH_2$	Reduced flavin adenine dinucleotide
hiPSC	human induced pluripotent stem cell
MM	Mitochondrial membrane
MPC	Mitochondrial pyruvate carrier
NADH	Reduced nicotinamide adenine dinucleotide
NRCM	Neonatal rat cardiomyocytes
PEP	Phosphoenolpyruvate
PC	Pyruvate carboxylase
ROS	Reactive oxygen species
SFN	Sulforaphane
TAC	Tricarboxylic acid cycle
TEM	Transmission electron microscopy
TMRM	Tetramethylrhodamine methyl ester

Native SFN and its cyclodextrin-stabilized variant (SFX-01) have regulatory approval for clinical studies in humans. The putative indications for clinical studies are broad, but actively mainly focus on neurological disorders (e.g. schizophrenia, autism, Alzheimer's disease) and cancer [5]. Here, finding an optimal therapeutic range in terms of free therapeutic plasma concentration remains challenging upon oral SFN administration. Although patients enrolled in clinical trials receive the same amount of SFN e.g. as a dietary supplement, observed plasma levels differed substantially between individuals [6]. In consequence, not only the beneficial, but also the unwanted side effects are difficult to predict and therefore remain the focus of ongoing preclinical trials in healthy probands [7]. So far, the reported number of unwanted side effects in clinical trials upon SFN administration was surprisingly low, given the potential of SFN to adduct to cellular protein. This is in contrast to studies performed in mice and rats, where SFN exhibited not only beneficial, but also harmful effects [8]. Although patients will perspectively receive SFN only for a limited time period, harmful effects that were observed in animal studies following a single high bolus application of SFN such as muscle weakness and even death, should not sink into oblivion [8].

Cardiac side effects are critical, if not the most critical kind of side effects that can be observed after administration of drug candidates in preclinical or later in clinical studies and thus, are still the main reason for late drug failure or withdrawal from the market [9,10]. Moreover, patients with prostate cancer, one of the future clinical indications of SFN therapy, often develop or suffer from cardiovascular disease simultaneously [11]. Over the past decades, we developed methods to investigate cardiotoxicity using three-dimensional, force-generating, spontaneously beating engineered heart tissue (EHT) prepared from different species [12–14] that virtually mimic a heart in the dish. EHTs are a suitable miniaturized platform to assess alterations in short-term and also long-term cardiomyocyte contractile performance under controlled sterile cell culture conditions [15,16].

The present study aimed on thoroughly characterizing the effects of acute and chronic SFN exposure on the contractile performance of EHTs derived from neonatal rat heart cells. SFN effects were investigated either acutely by short application of a spectrum of increasing SFN concentrations or where applicable one high SFN bolus concentration was applied. When administered chronically over the course of seven days, 1 μM was chosen as a low concentration that was within the range of detectable SFN plasma concentrations reported before in human trials [17,18]. SFN effects on EHT performance were investigated by analyzing spontaneous and electrically stimulated contraction patterns as a surrogate for unperturbed cardiomyocyte contractile function. Moreover, the direct impact of SFN on myofilament properties and Ca^{2+}-induced force development was investigated in chemically permeabilized cardiac mouse trabeculae exposed to SFN. The stretch-induced increase in force development was tested in response to chronic SFN exposure in EHTs. In addition, mitochondrial shape and function was analyzed by transmission electron microscopy and assessment of mitochondrial membrane potential alterations in response to SFN treatment. Contraction analyses and stress test by electrical pacing at high frequencies of chronically SFN-treated EHTs generated from human induced pluripotent stem cell (hiPSC)-derived cardiomyocytes was performed to confirm the relevance of the results for human cardiomyocytes and potentially patients.

2. Experimental

2.1. Materials

All chemicals, including SFN were purchased from Sigma-Aldrich (St. Louis, USA) if not stated otherwise. The Lactate-Glo™-kit was from Promega® (Walldorf, Germany).

2.2. Animals

The study was conducted in accordance with the guidelines for the care and use of laboratory animals as issued by the National Institutes of Health (Publication no. 85–23, revised 1985). Experimental procedures conformed to the German Law for the Protection of Animals. Neonatal rat cardiomyocytes from 0 to 3 day old Wistar rats (NRCMs) and hearts from adult male C57 BlackSwiss mice were isolated in the Institute of Experimental Pharmacology and Toxicology, University Medical Center Hamburg-Eppendorf.

2.3. Human induced pluripotent stem cells

Cardiomyocytes derived from human induced pluripotent stem cells (hiPSC) were differentiated from an in house hiPSC control line (UKEi001-A), which is registered at the European Human Stem Cell Registry (hPSCreg). The experimental utilisation of this cell line was approved by the Ethical Committee of the University Medical Center Hamburg-Eppendorf (Az. PV4798, 28.10.2014) with written informed consent.

2.4. Generation of EHTs and contraction analysis

EHTs were generated from either neonatal (P0–P3) rat or human induced pluripotent stem cell-derived cardiomyocytes (hiPSC-CMs) as previously described [14,15]. In brief, a reconstitution mix containing either 5×10^6/ml (NRCMs) or 8×10^6/ml (hiPSC-CMs) cells, 5 mg/ml fibrinogen, 3 U/ml thrombin and 2xDMEM (DMEM complemented with 20% horse serum, 2% penicillin/streptomycin) matching the volume of ingredients without nutrients was prepared. For hiPSC-CM-derived EHTs the Rho-kinase inhibitor Y-27632 (0.1%) was added to avoid cell death during casting. For each EHT, 97 μl of the reconstitution mix was separately added to 3 μl thrombin to avoid clotting of the entire master mix and pipetted into the agarose (2% in PBS) casting molds with PDMS racks (EHT Technologies GmbH, Germany) in a 24-well plate. EHTs were then incubated (37 °C, 7% CO_2, 40% O_2) for fibrin polymerization, before they were transferred to a new, medium-filled culture plate and kept for up to four weeks in culture. Culture medium (DMEM

with 10% horse serum, 1% penicillin/streptomycin, 10 μg/ml insulin, 33 μg/ml aprotinin) was changed every other day.

Auxotonic contractions were measured with a video-optical system (EHT Technologies GmbH, Germany) as previously described [12,19]. In brief, EHTs were placed in a gas-controlled chamber with a glass roof and videos were taken from above. A custom-made software (Consulting Team Machine Vision, CTMV, Pforzheim, Germany) automatically detected the individual EHT and calculated contraction parameters, like frequency, force, contraction and relaxation time that were given in a report after each measurement.

Isometric force measurement were performed in a converted organ bath. Four force transducers allowed measurements of one silicone rack with four EHTs in parallel. With a static counterpart, the preload of each EHT could be increased individually and stepwise (10 μm/step). The system was perfused with Tyrode's solution (in mM: NaCl 120, KCL 5.4, $MgCl_2$ 1.0, NaH_2PO_4 0.4, $NaHCO_3$ 22.6, glucose 5.0, $CaCl_2$ 0 for wash, 0.6 for submaximal, 1.8 for baseline), which was continuously aerated with carbogen (95% O_2, 5% CO_2) to ensure pH stability. For data evaluation, the LabChart® (ADInstruments, Spechbach, Germany) software was used.

2.5. Analyses of chemically permeabilized mouse trabeculae

For the analysis of force-Ca^{2+} relationships, cardiac trabeculae were prepared from the left ventricular endocardial surface of C57 BlackSwiss mice (N = 3) as reported before (Flenner et al., 2016). Ca^{2+}-sensitivity of skinned cardiac strips was evaluated using the permeabilized fiber test system 1400A from AuroraScientific. TritonX-100 permeabilized strips were fixed between a force transducer and a length controller. Trabeculae were stretched above slack length in activating solution ±30 μM SFN dissolved in 0.1% DMSO (pCa 4.5) at 15 °C until force development. They were then exposed to increasing Ca^{2+} concentrations from pCa9 to pCa4.5 in EGTA-buffer ±30 μM SFN dissolved in 0.1% DMSO. Force development was measured in each pCa solution. Data were analyzed using the Hill equation [20], with pCa50 as the free Ca^{2+} concentration, which yields 50% of the maximal force and nHill representing the Hill coefficient. The pCa50 represents the measure of myofilament Ca^{2+} sensitivity. Concentration response curves were fitted to the data points and force-pCa relationship comparison was done by using extrasum-of-squares F-test.

2.6. Pharmacological treatment of NRCMs and EHTs

NRCMs or EHTs were pretreated with vehicle (dimethylsulfoxide, DMSO) or sulforaphane (SFN; 0.1, 0.3, 1, 3, 10, 30 μM; 30 min pretreatment). Afterwards, medium was removed and NRCMs were fixed in 4% paraformaldehyde/PBS for 10 min for subsequent immunofluorescence analysis. 3–4 EHTs were pooled per sample and were lysed in lysis buffer (70 μl/EHT; 100 mM Tris-HCl pH 7.4; 150 mM NaCl; 1 mM EGTA; 1% Triton-X 100; Complete protease inhibitor cocktail) in a TissueLyser (Qiagen). Samples were either used for immunoprecipitation or SDS-polyacrylamide gel electrophoresis and immunoblot analysis.

2.7. Electron microscopy

EHTs were fixed in a mixture of 4% paraformaldehyde and 1% glutaraldehyde (Science Services, Germany) in 0.1 M phosphate buffer overnight at 4 °C. Samples were rinsed three times in 0.1 M sodium cacodylate buffer (pH 7.2–7.4) and osmicated using 1% osmium tetroxide in cacodylate buffer. Following osmication, the samples were dehydrated using ascending ethanol concentrations, followed by two rinses in propylene oxide. Infiltration of the embedding medium was performed by immersion in a 1:1 mixture of propylene oxide and Epon (Science Services, Germany), followed by neat Epon and hardening at 60 °C for 48 h. For light microscopy, semi-thin sections (0.5 μm) with longitudinal orientation were mounted on glass slides and stained for 1 min with 1% toluidine blue. For electron microscopy, ultra-thin sections (60 nm) were cut and mounted on copper grids and stained using uranyl acetate and lead citrate. Sections were examined and photographed using an EM902 (Zeiss) electron microscope equipped with a TRS 2K digital camera (A. Tröndle, Moorenweis, Germany).

2.8. Measurement of mitochondrial membrane potential

Mitochondrial membrane potential was analyzed using the selective mitochondrial dyes TMRM (tetramethylrhodamine methyl ester) and MitoTrackerGreen as a loading control. H9c2 cells were cultured in DMEM at 37 °C and 5% CO_2. For analysis cells were seeded on coated (1% of gelatine in DPBS) glass cover slips und treated with sulforaphane (1 μM SFN for chronic treatment and 3 μM or 30 μM SFN for acute treatment as indicated). Hydrogen peroxide (100 μM, 1 h) was applied to induce oxidative stress.

H9c2 were stained with 2,5 nM TMRM and 100 nM MitoTrackerGreen for 1 h. Samples were analyzed using a Leica TCS SP5 confocal microscope. TMRM was excited at 561 nm and emission was measured between 580 and 700 nm. MitoTrackerGreen was excited at 488 nm and emission was measured between 500 and 530 nm. For quantification at least 80 cells per condition and experiment were analyzed by computerized pixel counting.

The results represent the mean ± standard error, n = 4 biologically independent experiments.

2.9. Mitochondrial respiratory chain composition by blue native electrophoresis

NRCMs were cultured in 2D and exposed to vehicle (DMSO) or SFN (30 μM) for 6 h. Cells were pelleted and frozen in liquid nitrogen. Cell pellets were homogenized using a pre-cooled motor-driven glass/Teflon Potter-Elvehjem homogenizer at 2000 rpm and 40 strokes. Homogenates were centrifuged for 15 min at 600 g to remove nuclei, cell debris, and intact cells or fibers. Mitochondrial membranes were sedimented by centrifugation for 15 min at 22′000g. Mitochondrial-enriched pellets from 20 mg cells (wet weight) were resuspended in 35 μl solubilisation buffer (50 mM imidazole pH 7, 50 mM NaCl, 1 mM EDTA, 2 mM aminocaproic acid) and solubilized with 10 μl 20% (w/v) digitonin (Serva, Heidelberg). Samples were supplemented with 2.5 μl 5% Coomassie G250 in 500 mM aminocaproic acid and 5 μl 0.1% Ponceau S in 50% glycerol. Equal protein amounts of samples were loaded on top of a 3–18% acrylamide gradient gel (dimension 14 × 14 cm). After native electrophoresis in a cold chamber, blue-native gels were fixed in 50% (v/v) methanol, 10% (v/v) acetic acid, 10 mM ammonium acetate for 30 min and stained with Coomassie stain (0.025% Serva Blue G, 10% (v/v) acetic acid).

2.10. Lactate assay

For the lactate assay, the Lactate-Glo™-kit (Promega®) was applied according to manufacturers instructions. In brief, NRCMs were plated onto gelatin-coated (1% in DPBS) culture dishes (ø 3.5 cm) with a density of 0.3 × 10^6 cells/dish (37 °C, 7% CO_2). NRCMs were chronically treated with either DMSO, or SFN (1 μM, 10 μM). Prior to the lactate assay, cells were harvested and processed according to the manufacturers protocol. Bioluminescence of the samples was detected in duplicates with a luminometer (DLReady, Centro LB 960, Berthold Technologies). A standard curve was performed before each experiment (Supplemental Fig 1).

2.11. Redox assay

To determine the mitochondrial redox-state, a redox-sensitive red fluorescent protein, carrying a mitochondrial tag (rxRFP_mito) for organelle specificity [21], was cloned into an adeno-associated viral

vector 6 (AAV6). Depending on the surrounding environment, rxRFP_mito can change from a bright shining oxidized state, to a less fluorescent reduced one and thus, its intensity is a surrogate for the environmental redox state.

NRCMs were plated onto gelatin-coated (1% in DPBS) culture dishes (ø 3.5 cm) with a density of 0.3×10^6 cells/dish (37 °C, 7% CO_2). The cells were transduced (MOI 10,000) after adhering, which was usually completed two days after seeding. On day 3–4 post transduction rxRFP_mito was expressed stably and the mitochondrial redox-assay was performed. Therefore, living cells were monitored in EHT culture medium at room temperature with a confocal microscope (LSM, Zeiss; excitation: 540 nm, emission: 600 nm) under baseline conditions, followed by treatment with different concentrations of SFN (30 min), before they were reduced with DTT (dithiothreitol, 10 mM, 15 min), confirming functioning of the rxRFP_mito. Measurements were done in a non-cumulative way. Pictures were taken throughout the experiment and the pixel intensity was evaluated as a surrogate parameter for the redox state of the RFP with the ZEN light software (Zeiss). One value reflected the mean of about 30–35 cells.

2.12. Statistical analysis

Data were expressed as mean ± SEM. N-numbers and the individual statistical test are indicated for each figure. Statistical analyses were performed with the GraphPad Prism 5 software (GraphPad Software Inc. San Diego, CA, USA). P-values less than 0.05 were considered as significant.

3. Results

The study investigated the impact of acute or chronic SFN exposure on various aspects of key cardiomyocyte functions: systolic contraction, when the heart muscle contracts to pump blood into the body and diastolic relaxation, when the heart muscle relaxes to refill with blood. Thereby, treatment protocols involved initially exposure to a wider spectrum of acute SFN concentrations ranging between 0.1 and 30 μM. Due to the complexity of methods, subsequently, experiments were not performed for all SFN concentrations, but instead 30 μM was considered as an appropriate acute high bolus SFN concentration. As a chronic SFN intervention, exposure to 1 μM for the duration of 7 (2D) to three weeks (3D-EHTs) days in culture was used as this was within the concentration range of SFN plasma levels reported in human trials [17,18]. SFN exposure time for EHTs was increased compared to 2D cultures, to ensure full maturation and optimal contractile performance of the 3D heart muscle constructs.

3.1. Effects of acute SFN exposure on spontaneous cardiomyocyte contraction

SFN and its stabilized formulation SFX is in human clinical trials exploiting their therapeutic potential for the treatment of cancer and neurological disorders. The present study investigated the effect of SFN on cardiomyocyte contractile properties in an EHT-model, which allows sequential monitoring of contractile parameters of numerous EHTs. Initially, the acute response to cumulative concentrations of SFN on force, contraction, relaxation and beating frequency were assessed in DMEM (with 10 mmol/l HEPES (pH 7.4), 1% pen/strep) at 1.8 mM Ca^{2+},

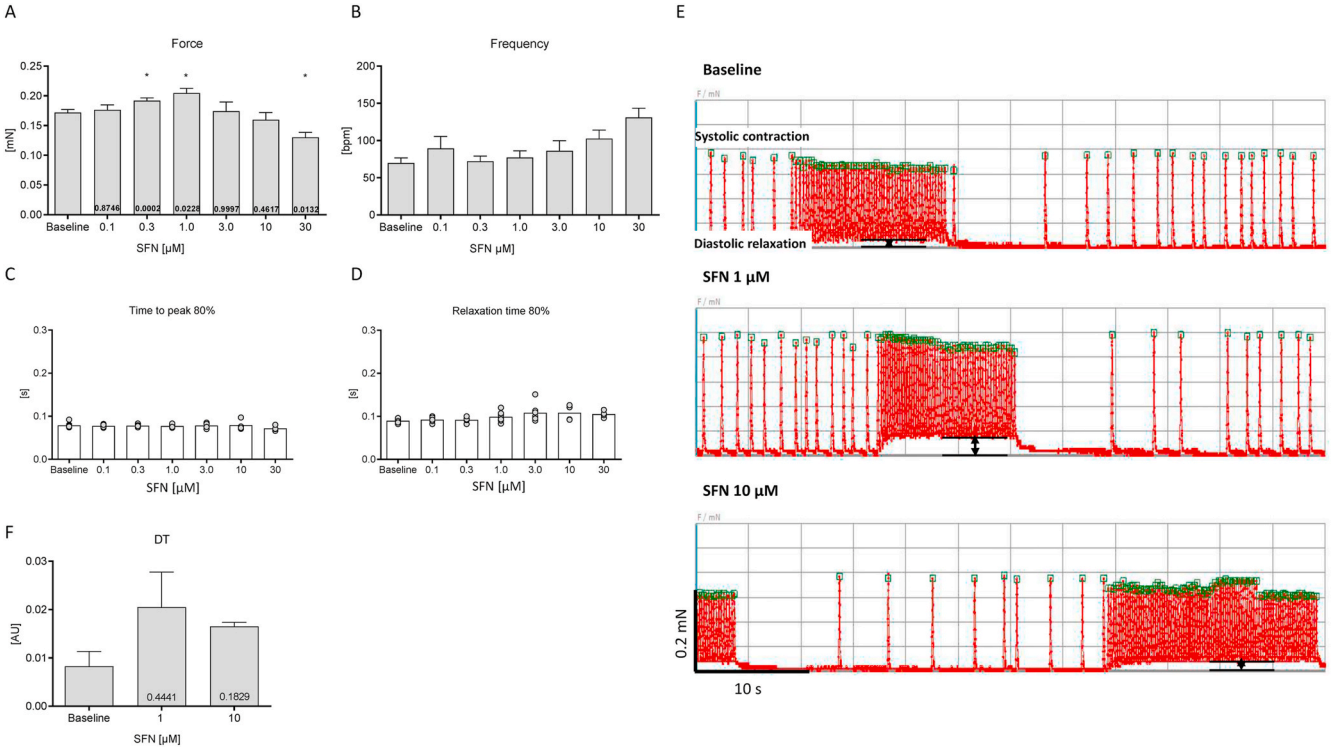

Fig. 1. Cumulative concentration-response-curve (CRC) of acute SFN treatment. Effects of 6 different concentrations of SFN on force (**A**), frequency (**B**), contraction (**C**) and relaxation time (**D**) of spontaneously beating rat EHTs in DMEM (with 10 mM HEPES (pH 7.4), 1% pen/strep, 1.8 mM Ca^{2+}) in the presence of epinephrine (50 nM) to enhance the likelihood of beating activity during recordings (60 s). Incubation time for each SFN exposure was 30 min. Original contraction pattern of a representative rat EHT during the concentration-response-curve. Rat EHTs show a spontaneous burst-like contraction pattern (**E** upper trace; Baseline). The initial slightly increased force of contraction by SFN at lower concentrations (1 μM) is shown in the middle trace (**E**). However, notably SFN also decreased diastolic length. To quantify this observation, the distance between the diastolic length during burst contractions and baseline length was assessed (**E**; arrows). This alteration is termed „diastolic tension (DT)" and is visualized as a bar chart in **F**. Data are presented in bar charts as mean values ± SEM (n = 7) or aligned dot plots. Each dot represents one analyzed EHT. Mean values are indicated as bars. *$P < 0.05$; One-way ANOVA followed by Dunnett's post hoc test. *P*-values are depicted in the respective bars.

considered as the maximum Ca^{2+} concentration (Fig. 1). EHTs derived from NRCMs beat spontaneously in a burst-like pattern [15]. Exposure of EHTs to 0.3 and 1 μM SFN significantly increased force. In contrast, a further increase in the SFN concentration to 30 μM significantly reduced force, suggesting adverse effects on cardiomyocyte function at higher SFN concentrations (Fig. 1A). However, the changes in force development in response to increasing SFN concentrations were paralleled by alterations in beating frequencies (Fig. 1B), thus not truly representing the impact of SFN on developed force that is known to be frequency-dependent (force-frequency relationship). Thus, a conclusive statement on the impact of SFN on force development can only be made during constant beating frequencies. There was no obvious impact of SFN on contraction and relaxation parameters detectable (Fig. 1C, D). When monitoring the original contraction traces of EHTs during cumulative SFN exposure, an observation was the impact of SFN on shortening diastolic length. This was reflected by the inability of the contraction peak to fully return to the diastolic length after the burst contraction period (Fig. 1E). This was visualized by measuring the distance between baseline contraction level (diastolic relaxation) and the shortened diastolic length reached during the burst (Fig. 1F).

3.2. Effects of acute SFN exposure on frequency-controlled cardiomyocyte contraction

To exclude frequency-effects on force, parts of the cumulative concentration response curve were repeated under frequency-controlled conditions (Fig. 2). To investigate whether the observed positive inotropic effect (increase in force) of SFN that was observed in Fig. 1 was mediated by a reduction in beating frequency, the experiment was repeated at submaximal Ca^{2+} concentrations and frequency-controlled conditions. To determine the optimal Ca^{2+} concentration for this experiment, a Ca^{2+} response curve was performed (Fig. 2A). Rat EHTs were then measured in Tyrode's solution at 0.6 mM and 2 Hz (Fig. 2B). Surprisingly, under these conditions, SFN exerted a negative inotropic effect (decrease in force; Fig. 2C), paralleled with a shortening of contraction time (time to peak contraction, Fig. 2D), while relaxation time (time to diastolic relaxation) was not affected (Fig. 2E). The maximal negative inotropic effect was observed at 3 μM SFN. Notably, the effect of SFN on force was only partially reversible upon wash-out (mean values ± SEM: Baseline 0.152 ± 0.009 mN; 3 μM 0.078 ± 0.005 mN; Wash 0.087 ± 0.010, n = 5; Fig. 2C).

3.3. Effects of acute SFN exposure on myofilament function

In order to investigate whether SFN directly impacts on myofilament function via modulation of the dynamic actin-myosin interaction thus crossbridge-cycling, force development depending on the presence of increasing exogenous Ca^{2+} concentrations (force-pCa^{2+}-relationship) were assessed. This was performed in detergent-permeabilized cardiac mouse trabeculae that solely contain the myofilament lattice without sarcolemma and cytosol. Trabeculae were exposed acutely to vehicle or 30 μM SFN. This high dose was chosen to investigate whether the negative inotropic response observed before in intact EHTs was due to direct modification of myofilament proteins. SFN treatment did not influence any prototypical myofilament properties such as maximal force (F_{max}), maximal force development (F_{max} related to cross-sectional area, CSA) nor the force-Ca^{2+} relationship. The Hill coefficient (nHill) as the indicator of cooperativity did not differ between the intervention groups (Fig. 3).

3.4. Effects of chronic SFN exposure on frequency-controlled cardiomyocyte contraction

To account for potential adverse cardiac side effects induced by SFN during chronic treatment as it would be expected to occur in patients during longterm treatment, rat EHTs were continuously exposed to 1 μM SFN from the first day of casting for up to three weeks and NRCMs in 2D culture for 7 days. This concentration was previously reported in human plasma after SFN administration [17,18]. As observed before, the SFN-treated EHTs developed lower forces throughout the entire culture time (measurements took place between day 5 and day 22), when compared to vehicle (DMSO; 0.1%) or untreated controls, with no

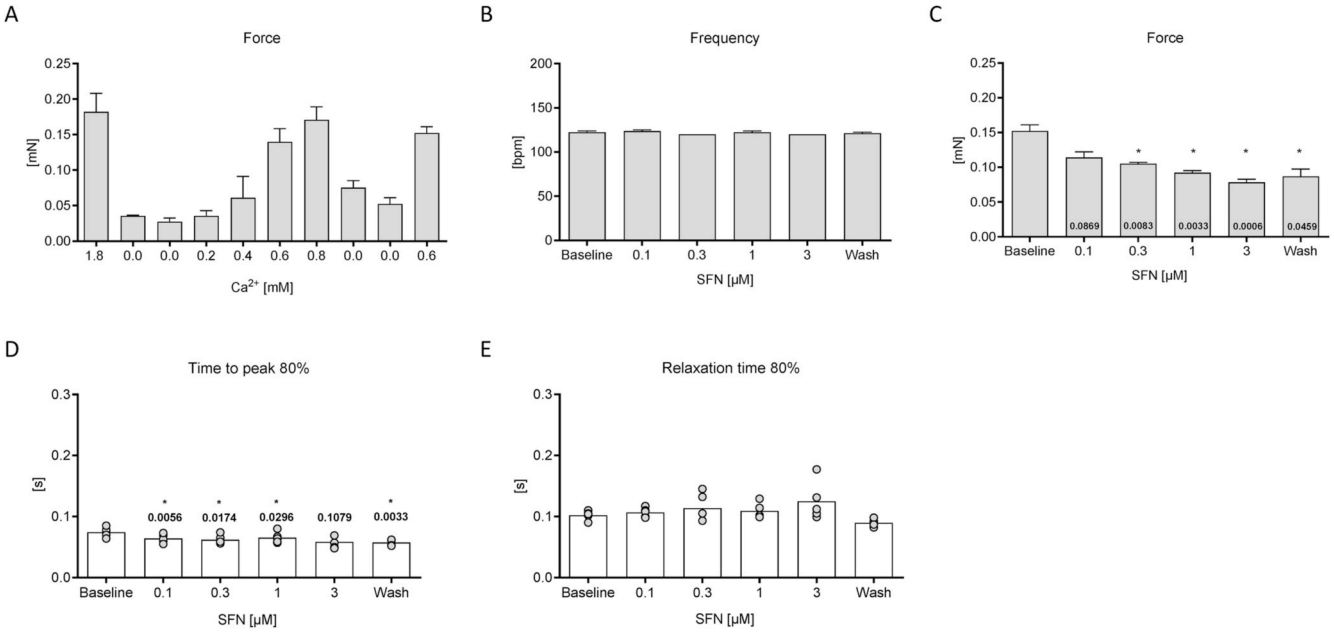

Fig. 2. Cumulative concentration-response curve (CRC) of SFN under frequency-controlled conditions. Construction of a Ca^{2+}-response curve (**A**) was important to determine a submaximal Ca^{2+} concentration for subsequent measurements. Effects of 6 different concentrations of SFN at a submaximal Ca^{2+} concentration (0.6 mM) on frequency (**B**), force (**C**), contraction (**D**) and relaxation time (**E**) of electrically stimulated (2 Hz) rat EHTs in Tyrode's solution. Incubation time was 30 min for each SFN concentration. Data are presented in bar charts with mean values ± SEM or aligned dot plots. Each dot represents one analyzed EHT. Mean values are indicated as bars. *$P < 0.05$, One-way ANOVA followed by Dunnett's post hoc test. *P*-values are depicted in the respective bars or above dots.

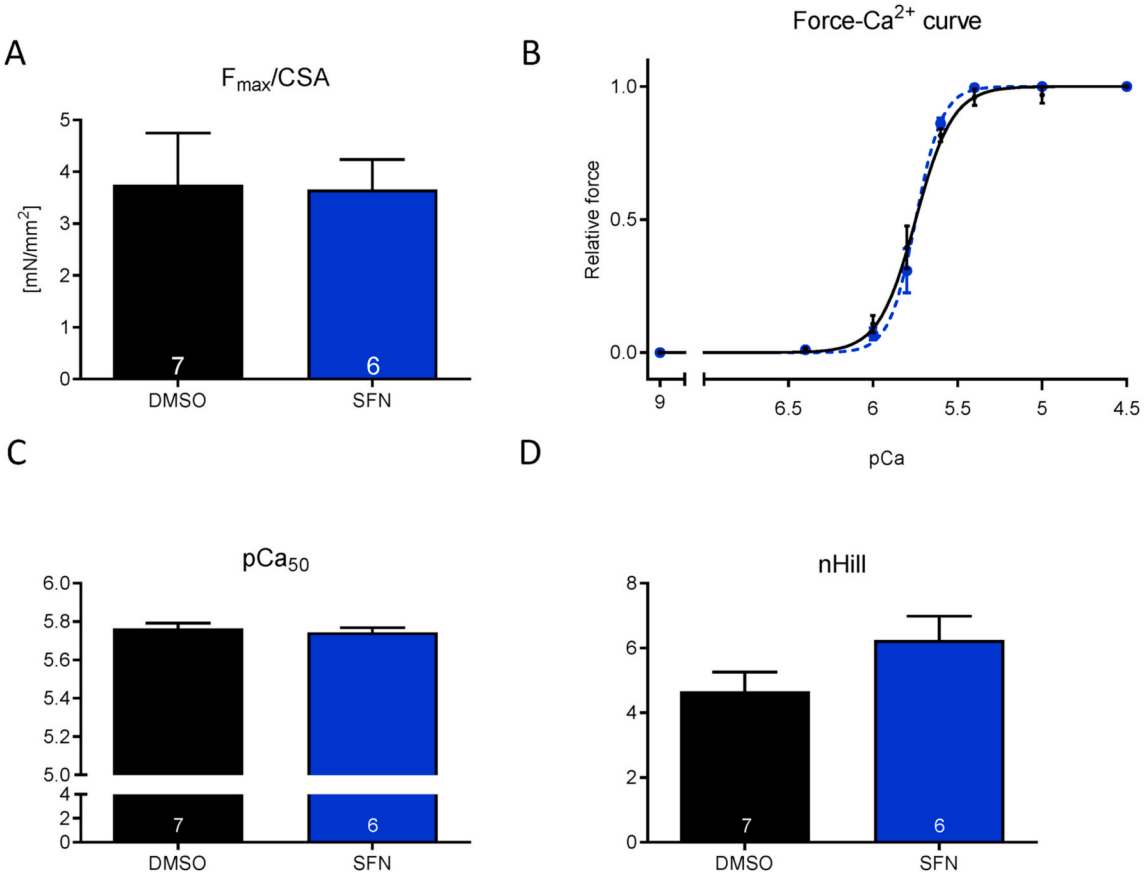

Fig. 3. Force-Ca^{2+} relationship of permeabilized cardiac muscle strips isolated from BlackSwiss mouse hearts in the presence and absence of SFN (30 μM). (**A**) Maximal force development (F_{max} related to cross-sectional area, CSA), (**B**) Force-Ca^{2+} concentration, (**C**) pCa_{50} as measure of myofilament Ca^{2+}-sensitivity, (**D**) nHill coefficient. Concentration response curves were fitted to the data points and curve comparison was done by using extra sum-of-squares F-test; n_{strips} = 6–7; N_{mice} = 3.

obvious changes in contraction kinetics (Supplemental Fig. 2A-C). EHTs were also measured under frequency-controlled conditions in culture medium during the plateau phase of force development to confirm the negative inotropic effect (mean values ± SEM: Control 0.112 ± 0.005 mN, n = 53; DMSO 0.123 ± 0.009 mN, n = 29; SFN 0.094 ± 0.007 n = 27; Fig. 4A). This difference was even more pronounced, when the experiment was repeated in Tyrode's solution (Ca^{2+} 1.8 mM, mean values ± SEM: Control 0.133 ± 0.011 mN, n = 8; DMSO 0.160 ± 0.011 mN, n = 8; SFN 0.097 ± 0.006 n = 7; Fig. 4B). Again, contraction kinetics were not affected by chronic SFN-treatment (Supplemental Fig. 2D and E).

3.5. Effects of chronic SFN exposure on stretch activation

Stretch activation, which is also known as the Frank-Starling mechanism (FSM), defines the positive correlation between heart muscle contraction and blood volume in the ventricles. Thereby, the increase in volume stretches the cardiac muscle fibers and triggers an increase in the force of contraction. This length-tension relationship occurs typically as a positive staircase over a wide range of mechanical stretch. This allows the heart to adapt to differences in physical exercise on a beat-to-beat base and an impairment is a typical clinical feature of heart failure patients [22].To study the effects of chronic SFN treatment on the length-tension relationship of cardiomyocytes, rat EHTs were continuously exposed to 1 μM SFN from the first day of casting for up to three weeks and then subjected to a stepwise increase in preload during isometric conditions (without alteration of muscle length) and the precise assessment of diastolic tension employed. First, the FSM was assessed at submaximal Ca^{2+} concentrations (0.6 mM) and electrical stimulation (2 Hz) by increasing the preload stepwise (20 μm/2 min). An original representative mechanogram of each group is depicted in Fig. 4E (Control: top panel, DMSO: middle panel, SFN: bottom panel). As exemplified for the control and DMSO mechanogramms at stage 4, the positive staircase phenomenon of the length-tension relationship was visible over a wide range of muscle length, as evidenced by the stepwise increase in force development without impact on diastolic tension. Compared to these controls, chronic SFN-treated EHTs revealed an unstable diastolic tension upon preload application as reflected by increasing diastolic tension. They reached the end of the FS staircase earlier, defined as three consecutive increases of the diastolic force paralleled with increases in systolic force, already after few preload adjustments (Fig. 4E, bottom panel). To rule out intergroup differences regarding the initial length of the EHTs prior to the experiment that would impact on the measurements, the slack length of all EHTs was determined. Surprisingly, this showed that EHTs after chronic exposure to SFN presented a longer slack length compared to vehicle and untreated controls (mean values ± SEM: Control 4.2 ± 0.2 mm, n = 8; DMSO 4.2 ± 0.2 mm, n = 8; SFN 4.9 ± 0.1 mm, n = 7; Fig. 4C). This further emphasized the impairment of the length-tension relationship in the chronic SFN treatment group (mean values ± SEM: Control 337 ± 38 μm, n = 7; DMSO 353 ± 25 μm, n = 8; SFN 191 ± 16 μm, n = 7; Fig. 4D).

3.6. Effects of chronic SFN exposure on mitochondrial shape and function

Cardiomyocytes contain a vast amount of mitochondria as they depend on mitochondrial ATP production to supply the energy demand of the heart muscle for continuous contraction. In the absence of an effect of SFN on the myofilaments, we next investigated whether SFN might impact on mitochondrial function and thus energy production as

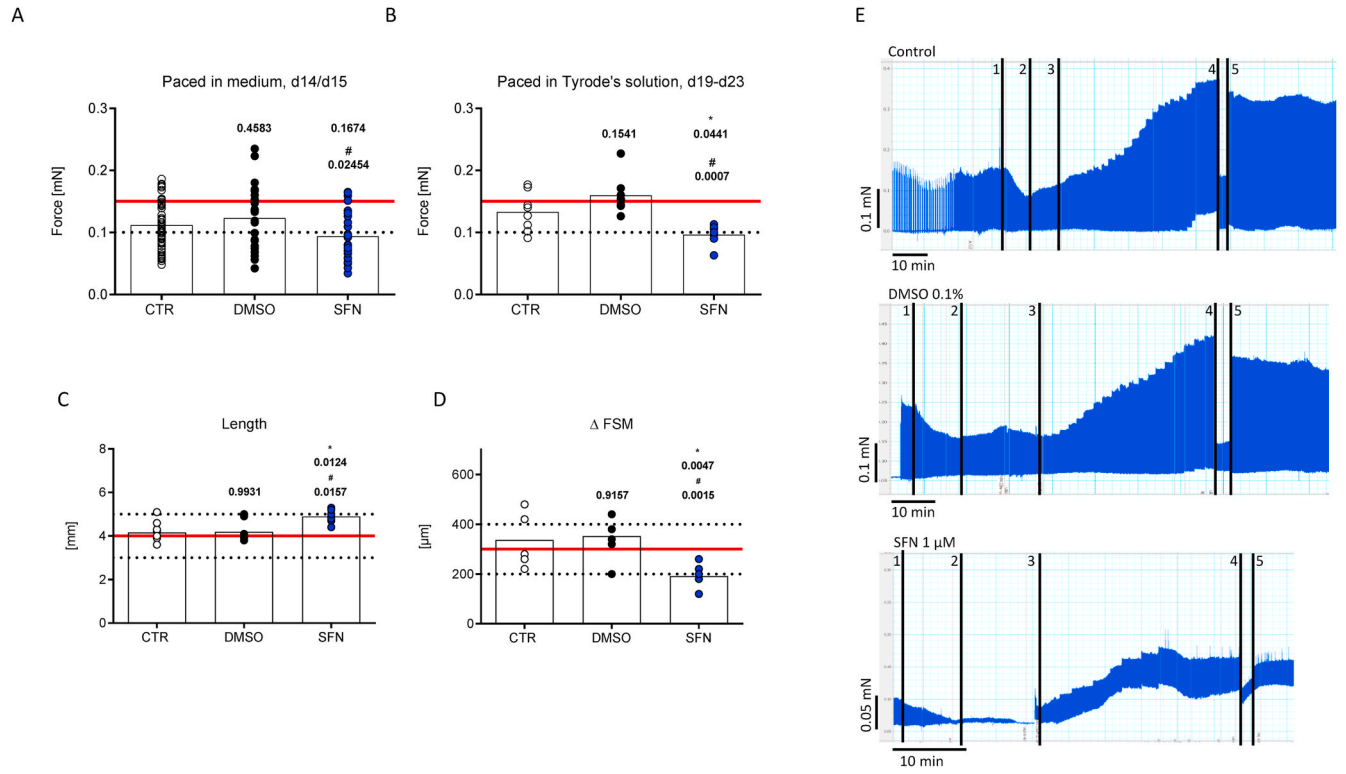

Fig. 4. Comparison of contractile forces during chronic SFN treatment and analysis of the Frank-Starling-mechanism (FSM). Rat EHTs were cultured for up to three weeks in medium, in the presence of 0.1% DMSO (vehicle control) or 1 μM SFN. To exclude frequency effects on force development, all groups were measured in the plateau phase (d14/15) under frequency-controlled conditions (2.5 Hz) in their respective culture medium (**A**). In addition, all EHTs were subjected to video-optical force measurements in Tyrode's solution (1.8 mM Ca^{2+}) and electrical stimulation (2 Hz; **B**), prior to measure stretch-activation in the Frank-Starling set-up (d19-23). The FSM of the EHTs was measured under isometrical force conditions. Representative mechanogram of EHTs from each group in Tyrode's solution and frequency-controlled contractions (2 Hz) are shown in **E** (upper panel control; middle panel DMSO 0.1%; bottom panel SFN 1 μM). Ca^{2+} was washed out (**E:1**), set to 0.6 mM (**E:2**), before the preload adjustment for the FSM started (**E:3**, 20 μm/2 min). After the FSM, EHTs were set back to slack length (**E:4**), before they were stretched to L_{80} (**E:5**). The slack length of all EHTs was determined before the experiment (**C**) and the total distance of stretch during the FSM was assessed (**D**). Hereby, each dot represents one analyzed EHT and bars indicate the mean values. EHTs were from two (**B-D**) or three (**A**) different batches. *,$^{\#}P < 0.05$, One-way ANOVA followed by Tukey's post hoc test. *P*-values are depicted above dots (*vs. control; $^{\#}$vs. DMSO).

this was described as the therapeutic mechanism exerted by SFN in cancer cells during an anti-cancer therapy [23]. We hypothesized that affecting mitochondrial function in cardiomyocytes that are highly depending on continuous energy supply by the mitochondria might lead to energy shortage and consequently affecting contractile properties.

EHTs that were cultured under control (untreated) or vehicle (DMSO) conditions or chronically exposed to SFN (1 μM; 7 days) were analyzed by transmission electron microscopy (TEM) to visualize overt ultrastructural alterations of the cardiomyocytes. Semi-thin sections revealed intergroup differences. Cardiomyocytes within EHTs that were untreated or treated with DMSO were nicely elongated along the force lines (Fig. 5A, left and middle). The cell density in SFN-treated EHTs was similar, however, cells appeared shorter, flat and rounded in the presence of SFN (Fig. 5A, right). Control EHTs showed well-defined sarcomeric structures with Z-discs and a large number of mitochondria perfectly intermingled with sarcomeres (Fig. 5B, left). DMSO-treated EHTs appeared less structured and showed inflated mitochondria with a darker matrix enlarged cisterns, potentially reflecting a higher respiration rate that is congruent with the observation of higher force development (Fig. 5B, middle). EHTs after chronic SFN treatment presented unstructured cellular organelles, with only a few misaligned sarcomeres and blurry Z-discs. Again, mitochondria were inflated and presented a whorled membrane appearance (Fig. 5B, right).

To investigate whether SFN alters the protein composition of the mitochondrial respiratory chain, mitochondrial membranes were isolated from NRCMs after vehicle (DMSO) or acute SFN treatment at a high bolus concentration (30 μM; 6 h) and analyzed by blue native polyacrylamide gel electrophoresis (BN-PAGE). Thereby, the distinct band pattern representing individual protein complexes and supercomplexes of the mitochondrial respiratory chain (S_{XL}, S_1, S_0, I, V, III, IV) were identified by comparing the pattern obtained from isolated bovine heart mitochondria (BHM; Fig. 5C). SFN did not alter the band pattern of the mitochondrial respiratory chain protein complexes and supercomplexes.

Pyruvate that is the end product of glycolysis is found at an important metabolic branch point. It is either transported into the mitochondria via the mitochondrial pyruvate carrier and metabolized by pyruvate carboxylase or by pyruvate dehydrogenase. Alternative to cytoplasmic-mitochondrial shuttling, pyruvate is reduced by lactate dehydrogenase to form lactate, allowing the regeneration of NAD^+.

To investigate the contribution of the mitochondria to the SFN-evoked contractile impairment, lactate levels were measured in vehicle (DMSO) and chronically SFN-treated (1 μM, 10 μM; 7 days) NRCMs in 2D culture. Exposure to SFN increased lactate levels compared to vehicle treated EHTs (Fig. 5D), suggesting a reduced cytoplasmic-mitochondrial pyruvate shuttling and instead reduction of pyruvate to lactate. Conversion of pyruvate by pyruvate dehydrogenase generates besides acetyl-CoA also $FADH_2$ and NADH, the latter two allowing the reduction of reactive oxygen species (ROS) that are a byproduct of the TAC.

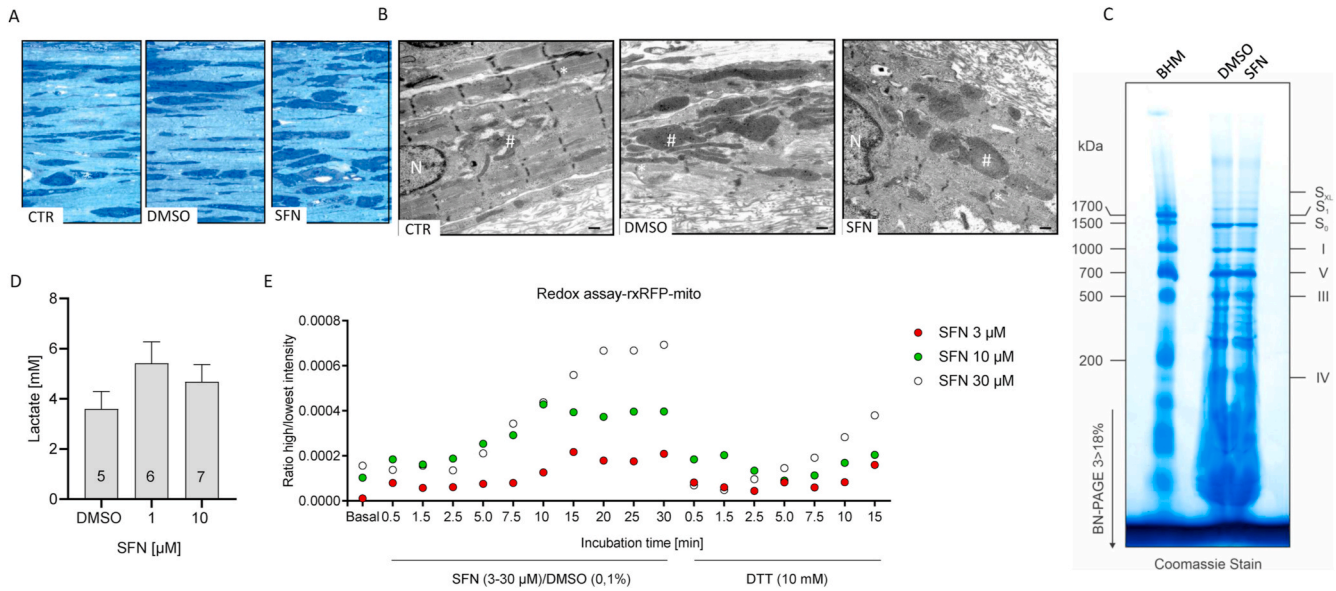

Fig. 5. Analyses of mitochondrial structure and function in chronically SFN-treated EHTs. The three groups were chronically treated (control, DMSO 0.1%, SFN 1 µM). EHTs were fixed and submitted to electron microscopy. Representing semi-thin (0.5 µm) sections of each group are depicted. (**A**) Structures in dark blue show cells, whereas light blue is considered as matrix proteins. (**B**) Electron microscopy revealed well structured sarcomeres with Z-discs in control EHTs. DMSO-treated EHTs seemed to be less structured with blown up mitochondria. In contrast to the control groups, SFN-treated EHTs appeared to be unstructured, with large swollen mitochondria. N: nucleus, *sarcomere/Z-disc, #mitochondria; scale bar 500 nm. (**C**) Analysis of the composition of the mitochondrial respiratory chain complexes in vehicle (DMSO) or SFN (30 µM; 6 h) treated NRCMs by blue native PAGE (BN-PAGE; 3–18%). The band pattern obtained from isolated bovine heart mitochondria (BHM) was used as a mass ladder. (**D**) Assessment of lactate production in 2D cultured NRCMs chronically treated (DMSO 0.1%, SFN 1 µM, 10 µM). (**E**) Assessment of mitochondrial reactive oxygen production in NRCMs transduced with AAV6-rxRFP exposed to SFN (3 µM, 10 µM, 30 µM) and alterations in fluorescence intensity recorded over 30 min. Reduction of rxRFP by addition of DTT (10 mM) to reverse sensor oxidation. (For interpretation of the references to colour in this figure legend, the reader is referred to the Web version of this article.)

3.7. Effects of SFN exposure on mitochondrial ROS production and membrane potential

Subsequently, the impact of SFN exposure on mitochondrial ROS production was assayed in NRCMs that were transduced with an adeno-associated viral vector (AAV6) encoding for a mitochondrial specific redox-sensitive red fluorescent protein (rxRFP_mito). Oxidation of the modified RFP induces disulfide formation, thereby increasing RFP fluorescence that can be detected. While basal fluorescence was low, exposure of transduced NRCMs acutely with high SFN concentrations (3–30 µM) led to a concentration-dependent increase in fluorescence intensity (Fig. 5E). Importantly, exposure to dithiothreitol (DTT) that reduces oxidative posttranslational modifications, reversed the SFN-induced fluorescence intensity, confirming that the increase in RFP signal upon SFN exposure was attributed to ROS-mediated RFP oxidation and not due to changes in NRCM shape.

An unspecific readout for mitochondrial integrity is the assessment of the mitochondrial membrane potential that has been described to decrease during enhanced ROS production [24,25]. The cardiomyocyte-like cell line H9c2 was exposed to the dyes tetramethylrhodamine methyl ester (TMRM) and MitoTrackerGreen as a loading control. Changes in the TMRM/MitoTrackerGreen ratio were measured after acute exposure of increasing high SFN concentrations, either in response to the positive control hydrogen peroxide (H_2O_2) or after a combination of SFN and H_2O_2. Acute exposure to SFN significantly reduced the mitochondrial membrane potential compared to the vehicle (DMSO) control (Fig. 6A; B, left panel). This effect was exacerbated by the combined exposure to SFN and H_2O_2 (Fig. 6A; B, right panel). Similarly, chronic exposure to a low SFN concentration for 7 days significantly reduced the mitochondrial membrane potential (Fig. 6C; D, left panel). Addition of H_2O_2 further reduced mitochondrial membrane potential (Fig. 6C, D, right panel).

3.8. Effects of chronic SFN exposure on frequency-controlled cardiomyocyte function with L-glutamine supplementation

Supplementation of the culture medium with an alternative substrate such as glutamine that bypasses the entrance of pyruvate into the TA-cycle could then potentially rescue the energy deficit evoked by SFN treatment. Also, L-glutamine has been described to protect mitochondria from damage by oxidants. Therefore, EHTs were exposed to chronic SFN in the presence and absence of L-glutamine (1%) supplementation in the medium. Auxotonic contraction analyses were performed in the force plateau phase under frequency-controlled conditions. The force was analyzed and expressed in percent of the respective group mean without L-glutamine. Surprisingly, although untreated control EHTs received an additional energy source in the culture medium, forces declined by approximately 50% compared to medium without L-glutamine. This effect was also observed in the vehicle DMSO group (force reduction for CTR -52% and DMSO -59%, respectively; Fig. 7A). Only in the presence of 1 µM SFN during culture, L-glutamine did not decrease forces. If at all, it even caused a slight increase in force of approximately 7% (Fig. 7A; Supplemental Figure 2F for kinetics). EHTs cultured with and without L-glutamine and SFN were subsequently analyzed by TEM. In both control groups, cell density seemed to be less in the presence of L-glutamine, although this effect was more pronounced in the untreated control group (Fig. 7B, left and middle). The cell density in SFN-treated EHTs appeared higher after supplementation with L-glutamine (Fig. 7B, right). Interestingly, TEM images did not intuitively reflect the observations on contractility. Whereas forces were substantially lower in untreated control EHTs cultured in the presence of L-glutamine, these EHTs showed not only well-defined sarcomeric structures with Z-discs, but also a large number of mitochondria perfectly intermingled with sarcomeres (Fig. 7C, left). In the DMSO group, L-glutamine supplementation was accompanied by blurred Z-discs, matrix condensation and whorled mitochondrial membranes (Fig. 7C, middle). Interestingly, the

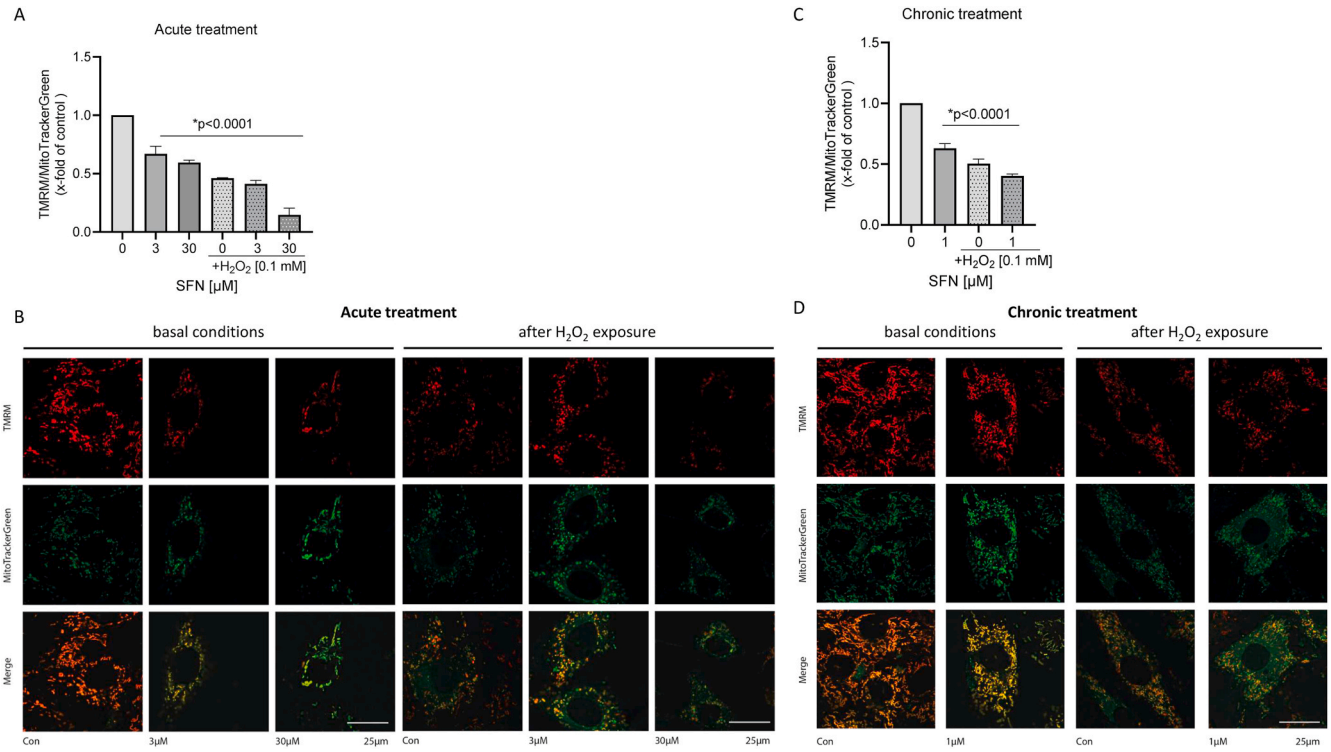

Fig. 6. Impact of acute and chronic SFN exposure on mitochondrial membrane potential. H9c2 cells were loaded with the selective mitochondrial dyes tetramethylrhodamine methyl ester (TMRM) and MitoTrackerGreen as a loading control. For acute treatment, cells were subsequently exposed for 1 h to SFN (3 µM, 30 µM) or hydrogen peroxide (H_2O_2; 100 µM, 1 h) or the combination. Alterations in mitochondrial membrane potential were expressed as the ratio of TMRM/MitoTrackerGreen fluorescence. (**A**) The bar chart represents the data summarized from 4 independent experiments of at least 80 cells per experiment. (**B**) Representative microscopic images for all conditions. For chronic treatment, H9c2 cells were chronically exposed to SFN (1 µM) in presence or absence of hydrogen peroxide (H_2O_2; 100 µM, 1 h). Cells were loaded with the selective mitochondrial dyes tetramethylrhodamine methyl ester (TMRM) and MitoTrackerGreen as a loading control. Alterations in mitochondrial membrane potential were expressed as the ratio of TMRM/MitoTrackerGreen fluorescence. **(C)** The bar chart represents the data summarized from 4 independent experiments of at least 80 cells per experiment. **(D)** Representative microscopic images for all conditions.

effect on the mitochondria in the SFN group was reversed in the presence of L-glutamine supplementation in the medium (Fig. 7C, right). This is even better visible in the close-up TEM-images of mitochondria and myofilaments in a side-by-side comparison between EHTs chronically exposed to SFN (Fig. 7D, left images) or with additional L-glutamine supplementation of the medium (Fig. 7D, right images). SFN exposure led to mitochondria with a more compact shape and a dark-appearing matrix with low abundance of contractile myofilaments. In contrast, L-glutamine supplementation of the culture medium improved mitochondrial shape and matrix appearance and also revealed a higher number of aligned myofibrils that corroborate the functional improvement.

3.9. Effects of chronic SFN exposure on hiPSC-cardiomyocyte function

Thus far, the study was performed in EHTs derived from neonatal rat heart cells not allowing immediate translation of the conclusions to a human background. Therefore, key experiments were repeated in EHTs prepared from human induced pluripotent stem cell-derived cardiomyocytes (hiPSC-CMs) of an inhouse control line. Human EHTs were generated and chronically exposed to either DMSO (0.1%) or SFN (1 µM) from the day of casting and maintained throughout the culture time for up to three weeks. Consequently, in the force plateau phase, EHTs were exposed to a stress test. EHTs were electrically stimulated at increasing beating rates in their respective culture medium (Ca^{2+} 1.8 mM), assuming that higher beating frequency would drive SFN-treated EHTs into an energy shortage, as time to restore ATP-depletion decreases at higher beating rates. Indeed, human EHTs developed lower forces compared to their vehicle DMSO-treated controls. Average peak height revealed 7% lower mean forces in the SFN group at physiological beating rates (1.5 Hz, Fig. 7E, left side; mean values ± SEM: DMSO 0.227 ± 0.006 mN, n = 9; SFN 0.214 ± 0.011 mN, n = 8). Interestingly, contraction time ($TTP_{80\%}$) was slightly reduced (mean values ± SEM: DMSO 0.141 ± 0.001 s, n = 9; SFN 0.135 ± 0.001 s, n = 8), whereas relaxation time tended to be increased (mean values ± SEM: DMSO 0.162 ± 0.003 s, n = 9; SFN 0.180 ± 0.005 s, n = 8), as it was previously observed in rat EHTs (Fig. 2D, E). The intergroup force difference increased at higher beating rates (4 Hz, Fig. 7E, right side; mean values ± SEM: DMSO 0.173 ± 0.005 mN, n = 9; SFN 0.136 ± 0.012 mN, n = 7), supporting the hypothesis of stepwise ATP-depletion as a consequence of higher energy demand. Overall, comparison of the average peaks showed not only the expected reduction of force and contraction kinetics upon frequency elevation, but also confirmed the decline in force production as a direct consequence of chronic SFN treatment in hiPSC-CMs-derived EHTs.

4. Discussion

This study aimed on elucidating the impact of acute and chronic SFN exposure on cardiomyocyte contractility. Although SFN and related compounds are already used in clinical trials, little is known about their impact on healthy and diseased myocardium.

A concentration response curve on spontaneously beating rat EHTs revealed a biphasic dose-response profile for SFN. Positive effects on inotropy could be observed until 1 µM, followed by a concentration-dependent negative inotropic effect at higher concentrations (3 µM, 10 µM, 30 µM, respectively). This biphasic-response was well in line with previous studies performed in other cell types, where SFN induced positive effects in the lower micromolar range in different cell culture models (e.g. HUVEC, PVC: angiogenesis or T24: migration [26,27]).

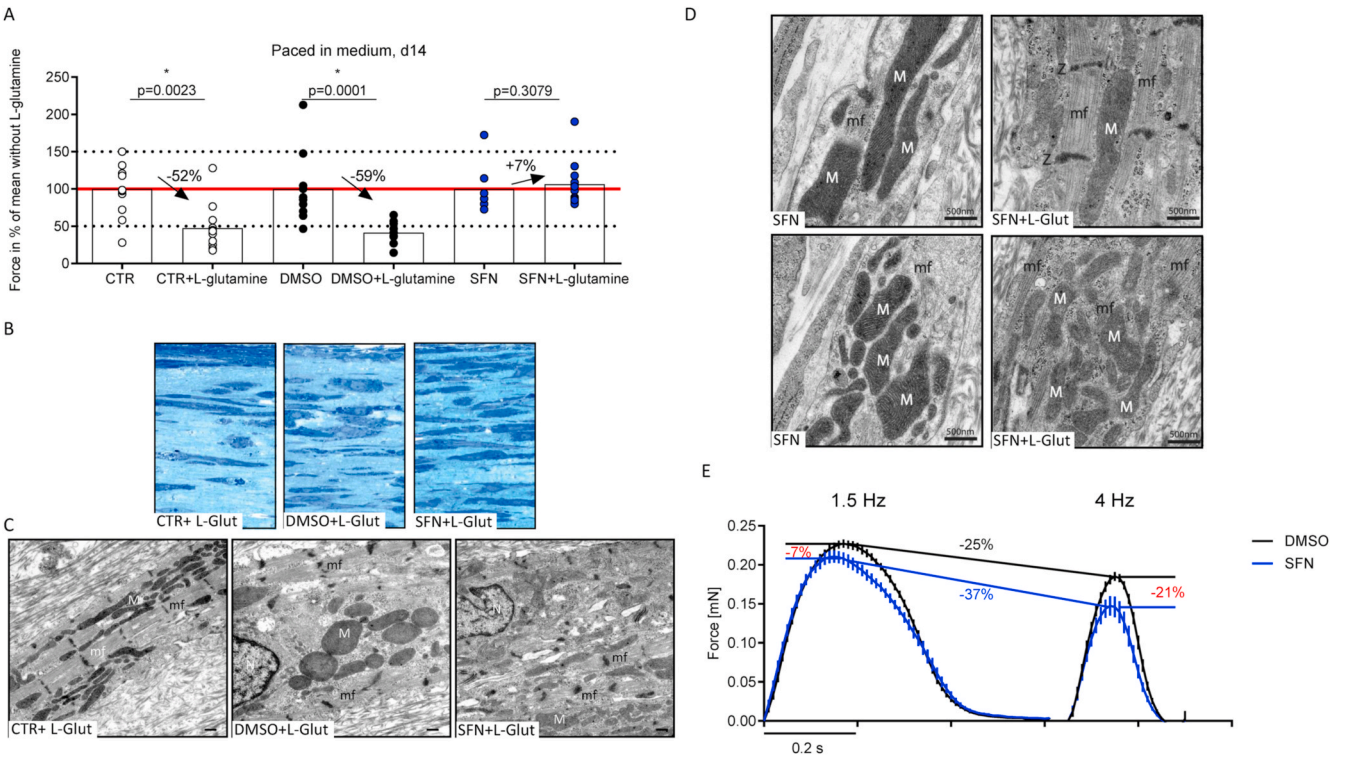

Fig. 7. Comparison of chronically treated rat EHTs in the presence and absence of L-glutamine. (**A**) To evaluate the effect of an additional energy source, all three groups were chronically treated (control, DMSO 0.1%, SFN 1 μM) and received L-glutamine (1%) supplementation. In the plateau-phase (d14) all groups were analyzed under frequency-controlled conditions (2 Hz). Force of contraction was calculated as percent of individual group mean without L-glutamine and statistics were performed for each group pair, respectively. Each dot represents one analyzed EHT and bars indicate mean values (n = 7–12). *$P < 0.05$, non-parametric *t*-test. *P*-values are depicted above dots. EHTs were then fixed and submitted to electron microscopy. Representing semi-thin (0.5 μm) sections of each group are depicted. (**B**) Structures in dark blue show cells, whereas light blue is considered as matrix proteins. (**C**) Electron microscopy revealed well structured sarcomeres with Z-discs accompanied by intermingled mitochondria in the CTR + L-glutamine group. In DMSO + L-glutamine treated EHTs, the mitochondria showed whorled membranes instead of clear cristae. In contrast to the control groups, SFN-treated EHTs showed in the presence of L-glutamine, a normalization of mitochondrial size, but Z-discs remained blurry. N: nucleus, mf: sarcomere/Z-disc, M: mitochondria; scale bar 500 nm. (**D**) Representative TEM-images showing a close-up of mitochondria and myofilaments in a direct side-by-side comparison after exposure to SFN or SFN supplemented with L-glutamine. N: nucleus, mf: myofilaments with sarcomere/Z-disc (Z), M: mitochondria; scale bar 500 nm. (**E**) Average peaks of chronically treated human EHTs. EHTs derived from human iPSC cardiomyocytes were chronically treated from the day of casting with either DMSO (0.1%) or SFN (1 μM). In the plateau phase of force development, EHTs were electrically stimulated with low (1.5 Hz) and high (4 Hz) frequencies. At a physiological frequency (1.5 Hz, left side), SFN-treated EHTs (blue peaks) exerted lower forces than DMSO-treated EHTs (black peaks). The difference in force development was accelerated when EHTs were paced with high frequencies (4 Hz, right side). (For interpretation of the references to colour in this figure legend, the reader is referred to the Web version of this article.)

Interestingly, even less than a doubling of the SFN-concentration showed the opposing effect on the studied parameters [26]. Taken together with our results, these observations argue for the necessity for intense plasma monitoring of the administered SFN in patients during therapy.

The negative effects observed on force of contraction could either be explained by a direct modulation of sarcomeric proteins or by an impact on cardiomyocyte metabolism and thus, ATP supply or by a combination of both. Interestingly, in animal studies, single high-dose SFN application led to muscle weakness [8], also suggesting an impact of SFN on muscle performance. Unfortunately, little, if nothing, is known about direct SFN-labelling of sarcomeric proteins. This is mainly due to the absence of SFN-specific antibodies and the difficulties in unbiased SFN detection methods. However, there are publications indicating that SFN downregulates βIII-tubulin in paclitaxel-resistant non-small lung cancer cells [28]. In cardiomyocytes, β-tubulins play a role in cardiac function [29]. In particular, βIII-tubulin is colocalized with Z-discs and mitochondria [30]. Thus, βIII-tubulin might contribute to the organization of sarcomeric proteins or as an inherent component of mitochondrial membranes might be involved in the correct positioning of the mitochondria into sarcomere vicinity, the site of high energy demand [31,32]. Interfering with βIII-tubulin expression could therefore also confer metabolic alterations in terms of mitochondrial function.

In the absence of a direct effect of SFN on myofilament function in chemically permeabilized mouse trabeculae, the effect of SFN on energy metabolism was investigated. Several proteins that regulate key steps of glycolysis and TAC have been described previously to be modulated by oxidants. As an example, pyruvate kinase (PKM) that regulates the rate limiting step of glycolysis has been shown to undergo functional cysteine modifications switching between catalytically inactive dimer and active tetramer formation [33]. This is interesting and could link SFN-mediated labelling of proteins to cardiomyocyte metabolism. SFN-mediated modulation of PKM activity would impact on phosphoenolpyruvic acid (PEP) conversion to pyruvate and lactate. Since PKM-isoforms (1 and 2) are responsible for this last step in glycolysis [34], they are important regulators of the TAC and consequently the gatekeepers regulating energy production. PKM1 is upregulated in tumor cells and promotes glycolysis and proliferation [35]. A common denominator of cardiomyocytes and tumor cells is their enormous energy demand [36]. Oxidative phosphorylation has the best ATP outcome, but is slow compared to other energy sources (e.g. glucose, amino acids). It is also oxygen-dependent. Consequently, the substrate for energetic supply can quickly shift upon rapid changes in ATP-demand or surrounding conditions, e.g. hypoxia; physical activity of cardiomyocytes or mitochondrial impairment in tumor cells [36]. Performing glycolysis in the presence of oxygen is known as the Warburg

effect [37,38]. In addition, immature cardiomyocytes prefer glycolysis even when oxygen supply is sufficient and thus, oxidative phosphorylation is a sign of maturation state [39].

Previous studies showed that the cardiomyocytes in the three dimensional EHT model were more mature than developmentally equally aged cells cultured in 2D, but still more comparable to the neonatal and not the adult state of the heart [12,40].

Investigating mice that only express one of the PKM isoforms, Morita and colleagues could nicely show that PKM1 mice were more prone to glycolysis and consumed less glutamine when compared to PKM2 mice [35]. With the hypothesis that chronically SFN-treated EHTs have an impaired PKM1 activity and therefore develop an energy shortage, they were substituted with L-glutamine to bypass the generation of pyruvate for entry into the TAC and thereby potentially rescue the energy deficit evoked by PKM inhibition. Indeed, chronically SFN-treated EHTs performed better in the presence of L-glutamine, which was in contrast to both control groups (Fig. 7A). The difference between SFN-treated EHTs and the controls might be explained by normally functioning glycolysis in untreated and DMSO-treated EHTs. However, also the EHTs of both control groups may have switched to glutaminolyses, when this substrate was more abundant, because glutamine metabolism is faster than oxidative phosphorylation and even glycolysis. Although it is faster, the ATP rate is the lowest in glutaminolyses compared to the other two metabolic alternatives. If EHTs switch from oxidative phosphorylation and glycolysis to glutaminolysis, the ATP outcome is anticipated to be much lower. Consequently, they would run into an energetic deficit and therefore develop lower forces. In contrast to that, when chronically treated with SFN, EHTs have an impaired glycolysis and thus, glutaminolyses could improve this. Hence, these EHTs would have more ATP and generate higher forces compared to SFN-treated EHTs in the absence of L-glutamine, which was the case in the present study.

The Frank-Starling mechanism of the heart, also known as length-dependent activation on the single cell level, is a well known adaptive mechanism that describes increasing force with increased preload [41,42]. Besides changes in Ca^{2+}-sensitivity and positioning of the sarcomeric proteins [43], more ATP needs to be produced to further support the increase in force. So again, the disturbed stretch-response after chronic SFN-treatment might point here to a metabolic deficit (Fig. 4D and E). If the energetic store is already exhausted at baseline levels, there is no further room for the development of higher forces, even though stretch is applied. In line with this observation, EHTs generated from hiPSC-CMs (hEHTs) revealed larger differences in force when paced at higher frequencies (Fig. 7D). Since ATP-recovery time is decreasing with increasing beating-rates, SFN-treated hEHTs potentially also suffer from insufficient energy supply. Interestingly, chemically permeabilized mouse trabeculae did not show any differences between SFN and vehicle treatment, which would rule out the contribution of sarcomeric proteins in the SFN-mediated deterioration of contractile performance. Furthermore, in this setting, ATP is supplied by the surrounding bath solution and does not need to be produced by the individual cell preparation. Thus, SFN effects on metabolism are covered in this experimental setting. In summary (GRAPHICAL ABSTRACT), the data from the present study reveal contractile and mitochondrial dysfunction of 2D and 3D-cultured cardiomyocytes from rat and human origin in response to acute and chronic SFN exposure. The data are of importance in the light of ongoing clinical trials in cancer patients and highlight the importance of monitoring cardiac function during administration of SFN at least in patients with existing cardiovascular co-morbidities.

5. Conclusion

This study provides evidence that SFN affects cardiac contractile function, most likely by interfering with cardiomyocyte metabolism and thus, ATP supply. This represents the desired pharmacological mechanism of SFN-action on cell types with high-energy demand such as tumor cells. However, metabolic capping could cause severe adverse cardiac side effects during SFN therapy in cancer patients, especially in those with a pre-existing cardiac co-morbidity. Therefore the results of the present study should raise awareness for the importance of controlling SFN plasma levels and cardiac function in patients.

Author contribution statement

AR designed the study, performed experiments, analysed data, wrote the manuscript. FF performed experiments in chemically permeabilized mouse trabeculae. TB assessed and analyzed mitochondrial membrane potential. JR performed cell culture experiments. MS performed TEM analyses. JM performed BN-PAGE. IW performed BN-PAGE. BMU provided the hiPSC cell line. BK performed hiPSC-cardiomyocyte differentiation. JU prepared NRCMs. AP performed cell culture experiments and assessment of lactate formation. KL assessed and analyzed mitochondrial membrane potential. TE provided the hiPSC cell line. AH provided the hiPSC cell line. FC designed the study, performed experiments, analysed data, wrote the manuscript. All authors proof-read the manuscript and provided intellectual input.

Declaration of competing interest

None.

Funding information

This study was supported by the Deutsche Forschungsgemeinschaft (DFG grant CU 53/2–1; CU 53/5–1, ED 298/1-1), the Werner Otto Stiftung (8/89; 7/92), the Deutsches Zentrum für Herz-Kreislauf-Forschung (DZHK), the Deutsche Stiftung für Herzforschung.

Acknowledgments

None.

Appendix A. Supplementary data

Supplementary data to this article can be found online at https://doi.org/10.1016/j.redox.2021.101951.

References

[1] A. Vanduchova, P. Anzenbacher, E. Anzenbacherova, Isothiocyanate from broccoli, sulforaphane, and its properties, J. Med. Food 22 (2) (2019) 121–126, https://doi.org/10.1089/jmf.2018.0024.

[2] X. Lv, G. Meng, W. Li, et al., Sulforaphane and its antioxidative effects in broccoli seeds and sprouts of different cultivars, Food Chem. 316 (2020) 126216, https://doi.org/10.1016/j.foodchem.2020.126216.

[3] R.T. Ruhee, S. Ma, K. Suzuki, Protective effects of sulforaphane on exercise-induced organ damage via inducing antioxidant defense responses, Antioxidants 9 (2) (2020) 136, https://doi.org/10.3390/antiox9020136.

[4] M.J. Goodfellow, A. Borcar, J.L. Proctor, T. Greco, R.E. Rosenthal, G. Fiskum, Transcriptional activation of antioxidant gene expression by Nrf2 protects against mitochondrial dysfunction and neuronal death associated with acute and chronic neurodegeneration, Exp. Neurol. 328 (2020) 113247, https://doi.org/10.1016/j.expneurol.2020.113247.

[5] clinicaltrialsgov. https://www.clinicaltrials.gov/ct2/results?recrs=&cond=&term=sulforaphane&cntry=&state=&city=&dist=.

[6] J. Sun, C.S. Charron, J.A. Novotny, B. Peng, L. Yu, P. Chen, Profiling glucosinolate metabolites in human urine and plasma after broccoli consumption using non-targeted and targeted metabolomic analyses, Food Chem. 309 (2020) 125660, https://doi.org/10.1016/j.foodchem.2019.125660.

[7] A.H. Zolnourian, S. Franklin, I. Galea, D.O. Bulters, Study protocol for SFX-01 after subarachnoid haemorrhage (SAS): a multicentre randomised double-blinded, placebo controlled trial, BMJ Open 10 (3) (2020), e028514, https://doi.org/10.1136/bmjopen-2018-028514.

[8] Y. Yagishita, J.W. Fahey, A.T. Dinkova-Kostova, T.W. Kensler, Broccoli or sulforaphane: is it the source or dose that matters? Molecules 24 (19) (2019) https://doi.org/10.3390/molecules24193593.

[9] W. Haverkamp*, The potential for QT prolongation and pro-arrhythmia by non-anti-arrhythmic drugs: clinical and regulatory implications Report on a Policy

Conference of the European Society of Cardiology, Cardiovasc. Res. 47 (2) (2000) 219–233, https://doi.org/10.1016/S0008-6363(00)00119-X.
[10] A. Eder, I. Vollert, A. Hansen, T. Eschenhagen, Human engineered heart tissue as a model system for drug testing, Adv. Drug Deliv. Rev. 96 (2016) 214–224, https://doi.org/10.1016/j.addr.2015.05.010.
[11] M.S. Anker, S. von Haehling, U. Landmesser, A.J.S. Coats, S.D. Anker, Cancer and heart failure-more than meets the eye: common risk factors and co-morbidities, Eur. J. Heart Fail. 20 (10) (2018) 1382–1384, https://doi.org/10.1002/ejhf.1252.
[12] A. Hansen, A. Eder, M. Bönstrup, et al., Development of a drug screening platform based on engineered heart tissue, Circ. Res. 107 (1) (2010) 35–44, https://doi.org/10.1161/CIRCRESAHA.109.211458.
[13] Stöhr A, Friedrich FW, Flenner F, et al. Contractile abnormalities and altered drug response in engineered heart tissue from Mybpc3-targeted knock-in mice. J. Mol. Cell. Cardiol.. Published online July 26, 2013. doi:10.1016/j.yjmcc.2013.07.011.
[14] I. Mannhardt, K. Breckwoldt, D. Letuffe-Brenière, et al., Human engineered heart tissue: analysis of contractile force, Stem cell reports 7 (1) (2016) 29–42, https://doi.org/10.1016/j.stemcr.2016.04.011.
[15] A. Eder, A. Hansen, J. Uebeler, et al., Effects of proarrhythmic drugs on relaxation time and beating pattern in rat engineered heart tissue, Basic Res. Cardiol. 109 (6) (2014) 436, https://doi.org/10.1007/s00395-014-0436-7.
[16] F. Jacob, A.Y. Yonis, F. Cuello, et al., Analysis of tyrosine kinase inhibitor-mediated decline in contractile force in rat engineered heart tissue, PloS One 11 (2) (2016), e0145937, https://doi.org/10.1371/journal.pone.0145937.
[17] A. Langston-Cox, D. Anderson, D.J. Creek, K. Palmer, E.M. Wallace, S.A. Marshall, Measuring sulforaphane and its metabolites in human plasma: a high throughput method, Molecules 25 (4) (2020), https://doi.org/10.3390/molecules25040829.
[18] J.W. Fahey, K.L. Wade, S.L. Wehage, et al., Stabilized sulforaphane for clinical use: phytochemical delivery efficiency, Mol. Nutr. Food Res. 61 (4) (2017), https://doi.org/10.1002/mnfr.201600766.
[19] A. Eder, I. Vollert, A. Hansen, T. Eschenhagen, Human engineered heart tissue as a model system for drug testing, Adv. Drug Deliv. Rev. 96 (2016) 214–224, https://doi.org/10.1016/j.addr.2015.05.010.
[20] T.L. Hill, E. Eisenberg, L. Greene, Theoretical model for the cooperative equilibrium binding of myosin subfragment 1 to the actin-troponin-tropomyosin complex, Proc. Natl. Acad. Sci. Unit. States Am. 77 (6) (1980) 3186–3190, https://doi.org/10.1073/pnas.77.6.3186.
[21] Y. Fan, H.W. Ai, Development of redox-sensitive red fluorescent proteins for imaging redox dynamics in cellular compartments, Anal. Bioanal. Chem. 408 (11) (2016) 2901–2911, https://doi.org/10.1007/s00216-015-9280-3.
[22] V. Sequeira, J. van der Velden, Historical perspective on heart function: the Frank-Starling Law, Biophys Rev 7 (4) (2015) 421–447, https://doi.org/10.1007/s12551-015-0184-4.
[23] G.H. Jo, G.-Y. Kim, W.-J. Kim, K.Y. Park, Y.H. Choi, Sulforaphane induces apoptosis in T24 human urinary bladder cancer cells through a reactive oxygen species-mediated mitochondrial pathway: the involvement of endoplasmic reticulum stress and the Nrf2 signaling pathway, Int. J. Oncol. 45 (4) (2014) 1497–1506, https://doi.org/10.3892/ijo.2014.2536.
[24] D.B. Zorov, M. Juhaszova, S.J. Sollott, Mitochondrial ROS-induced ROS release: an update and review, Biochim. Biophys. Acta Bioenerg. 1757 (5–6) (2006) 509–517, https://doi.org/10.1016/j.bbabio.2006.04.029.
[25] J.M. Suski, M. Lebiedzinska, M. Bonora, P. Pinton, J. Duszynski, M.R. Wieckowski, Relation between Mitochondrial Membrane Potential and ROS Formation, 2012, pp. 183–205, https://doi.org/10.1007/978-1-61779-382-0_12.
[26] Y. Bao, W. Wang, Z. Zhou, C. Sun, in: D. Nie (Ed.), Benefits and Risks of the Hormetic Effects of Dietary Isothiocyanates on Cancer Prevention, PLoS One, 2014, e114764, https://doi.org/10.1371/journal.pone.0114764, 9(12).
[27] J. Jodynis-Liebert, M. Kujawska, Biphasic dose-response induced by phytochemicals: experimental evidence, J. Clin. Med. 9 (3) (2020), https://doi.org/10.3390/jcm9030718.
[28] Y. Wang, Y. Zhou, Z. Zheng, J. Li, Y. Yan, W. Wu, Sulforaphane metabolites reduce resistance to paclitaxel via microtubule disruption, Cell Death Dis. 9 (11) (2018) 1134, https://doi.org/10.1038/s41419-018-1174-9.
[29] L.A. Aquila-Pastir, N.R. DiPaola, R.G. Matteo, N.G. Smedira, P.M. McCarthy, C. S. Moravec, Quantitation and distribution of β-tubulin in human cardiac myocytes, J. Mol. Cell. Cardiol. 34 (11) (2002) 1513–1523, https://doi.org/10.1006/jmcc.2002.2105.
[30] R. Guzun, M. Karu-Varikmaa, M. Gonzalez-Granillo, et al., Mitochondria–cytoskeleton interaction: distribution of β-tubulins in cardiomyocytes and HL-1 cells, Biochim. Biophys. Acta Bioenerg. 1807 (4) (2011) 458–469, https://doi.org/10.1016/j.bbabio.2011.01.010.
[31] M. Carré, N. André, G. Carles, et al., Tubulin is an inherent component of mitochondrial membranes that interacts with the voltage-dependent anion channel, J. Biol. Chem. 277 (37) (2002) 33664–33669, https://doi.org/10.1074/jbc.M203834200.
[32] K. Tepp, K. Mado, M. Varikmaa, et al., The role of tubulin in the mitochondrial metabolism and arrangement in muscle cells, J. Bioenerg. Biomembr. 46 (5) (2014) 421–434, https://doi.org/10.1007/s10863-014-9579-3.
[33] Masaki S, Hashimoto K, Kihara D, Tsuzuki C, Kataoka N, Suzuki K. The cysteine residue at 424th of pyruvate kinase M2 is crucial for tetramerization and responsiveness to oxidative stress. Biochem. Biophys. Res. Commun.. Published online April 2020. doi:10.1016/j.bbrc.2020.03.182.
[34] W.J. Israelsen, M.G. Vander Heiden, Pyruvate kinase: function, regulation and role in cancer, Semin. Cell Dev. Biol. 43 (2015) 43–51, https://doi.org/10.1016/j.semcdb.2015.08.004.
[35] M. Morita, T. Sato, M. Nomura, et al., PKM1 confers metabolic advantages and promotes cell-autonomous tumor cell growth, Canc. Cell 33 (3) (2018) 355–367, https://doi.org/10.1016/j.ccell.2018.02.004, e7.
[36] A. Karlstaedt, W. Schiffer, H. Taegtmeyer, Actionable metabolic pathways in heart failure and cancer—lessons from cancer cell metabolism, Front Cardiovasc Med 5 (2018), https://doi.org/10.3389/fcvm.2018.00071.
[37] M. Potter, E. Newport, K.J. Morten, The Warburg effect: 80 years on, Biochem. Soc. Trans. 44 (5) (2016) 1499–1505, https://doi.org/10.1042/BST20160094.
[38] M.V. Liberti, J.W. Locasale, The Warburg effect: how does it benefit cancer cells? Trends Biochem. Sci. 41 (3) (2016) 211–218, https://doi.org/10.1016/j.tibs.2015.12.001.
[39] G.D. Lopaschuk, J.S. Jaswal, Energy metabolic phenotype of the cardiomyocyte during development, differentiation, and postnatal maturation, J. Cardiovasc. Pharmacol. 56 (2) (2010) 130–140, https://doi.org/10.1097/FJC.0b013e3181e74a14.
[40] B.M. Ulmer, A. Stoehr, M.L. Schulze, et al., Contractile work contributes to maturation of energy metabolism in hiPSC-derived cardiomyocytes, Stem Cell Reports 10 (3) (2018) 834–847, https://doi.org/10.1016/j.stemcr.2018.01.039.
[41] Y. Ait-Mou, K. Hsu, G.P. Farman, et al., Titin strain contributes to the Frank–Starling law of the heart by structural rearrangements of both thin- and thick-filament proteins, Proc. Natl. Acad. Sci. Unit. States Am. 113 (8) (2016) 2306–2311, https://doi.org/10.1073/pnas.1516732113.
[42] O. Lookin, Y. Protsenko, Length-dependent activation of contractility and Ca-transient kinetics in auxotonically contracting isolated rat ventricular cardiomyocytes, Front. Physiol. 10 (2019), https://doi.org/10.3389/fphys.2019.01473.
[43] P.P. de Tombe, R.D. Mateja, K. Tachampa, Y. Ait Mou, G.P. Farman, T.C. Irving, Myofilament length dependent activation, J. Mol. Cell. Cardiol. 48 (5) (2010) 851–858, https://doi.org/10.1016/j.yjmcc.2009.12.017.